N94-24145

Computation of turbulent flows over backward and forward-facing steps using a near-wall Reynolds stress model

By S. H. Ko

1. Motivation and objectives

Separation and reattachment of turbulent shear layers is observed in many important engineering applications, yet it is poorly understood. This has motivated many studies on understanding and predicting the processes of separation and reattachment of turbulent shear layers. Both of the situations in which separation is induced by adverse pressure gradient, or by discontinuities of geometry, have attracted attention of turbulence model developers. Formulation of turbulence closure models to describe the essential features of separated turbulent flows accurately is still a formidable task.

The present report describes computations of separated flows associated with sharp-edged bluff bodies. For the past two decades, the backward-facing step flow, the simplest separated flow, has been a popular test case for turbulence models. Detailed studies on the performance of many turbulence models, including two-equation turbulence models and Reynolds stress models, for flows over steps can be found in the papers by Thangam & Speziale (1992) and Lasher & Taulbee (1992). These studies indicate that almost all the existing turbulence models fail to accurately predict many important features of backstep flow such as reattachment length, recovery rate of the redeveloping boundary layers downstream of the reattachment point, streamlines near the reattachment point, and the skin friction coefficient.

An elliptic relaxation model was proposed by Durbin (1991) to represent inhomogeneous effects near the surface of wall-bounded shear flows. This model obviated the need for *ad hoc* eddy viscosity damping functions in the near wall region. After showing that the elliptic relaxation approach was successful in simple flows such as channel flow and flat plate, attached boundary layers, the model was extended to a full near-wall Reynolds stress model (Durbin, 1993) (hereinafter NRSM).

Using the NRSM, Ko & Durbin (1993) computed the massively separated boundary layer experiment of Simpson *et al.* (1981) and found that the new model was able to produce a reasonable separated flow. However, due to ambiguities in the experimented flow condition, it was difficult to draw any conclusion on the model performance. Therefore, it is necessary to have a well-defined test case with clear-cut boundary conditions in order to isolate phenomena which are directly related to the turbulence model. In addition, Direct Numerical Simulation (hereinafter DNS) data (Le & Moin, 1993) has recently become available for a low Reynolds number backward-facing step flow.

The main objectives of the present study are to calculate flows over backward-
and forward-facing steps using the NRSM and to make use of the newest DNS data
for detailed comparison. This will give insights for possible improvement of the
turbulence model.

2. Accomplishments

As stated previously, the NRSM is capable of describing near-wall effects without
using *ad hoc* damping functions. The model utilizes elliptic differential equations to
account for non-local wall blocking effects. The model equations will not be listed
here. Detailed discussion of the model and its boundary conditions can be found in
Durbin (1991, 1993); our computational methods are described in Ko (1993).

2.1. Turbulent flows over backward-facing steps

Turbulent backward-facing step flows were computed for the experimental con-
ditions reported by three different groups: Kim *et al.* (1980, KKJ), Driver &
Seegmiller (1985, DS), and Jovic & Driver (1993, JD). DNS data of Le & Moin
(1993, LM) is used for detailed comparison of the Reynolds-stress budgets. Table
1 summarizes flow conditions of the test cases. It is desirable to have a small ex-
pansion ratio E_r to minimize freestream pressure gradient effects (Narayanan *et al.*,
1974): the KKJ case is subjected to a significant freestream pressure gradient due
to the large expansion ratio; the other two cases are not. Notice also that JD's
experiment and LM's DNS have identical flow conditions; in fact, JD's experiment
was performed in order to verify the accuracy of the DNS. The predicted reattach-
ment lengths X_r for all cases are in very good agreement with the measured X_r,
although slightly underestimated.

Group	E_r $= H_1/H_2$	Re_h $= U_o H/\nu$	δ^*/h	Meas. X_r	Pred. X_r
Kim *et al.*	1.5	45,000	0.03867	7	6.8
Driver and Seegmiller	1.125	37,500	0.2	6.3	6.1
Jovic and Driver	1.2	5,100	0.19	6	5.4
Le and Moin	1.2	5,100	0.19	6	-

Table 1.   Test cases for backward-facing step flows

For all the turbulent backward-facing flow problems, the computational domain
extended from the step ($x = 0$) to $40H$, where H is the step height. This long
domain ensures that the zero-normal gradient boundary condition, $\partial/\partial x = 0$, is
appropriate for all flow variables at the outlet of the domain. It is often observed
that a shorter computational domain results in unstable and/or unsteady solutions
for separated flow problems.

Along the inlet of the domain, profiles of all the flow variables were specified.
Since the inlet is at the step, which is the onset of sudden changes, the whole
computation procedure and the resulting flowfield are sensitive to the specified
inlet conditions. Therefore, it is very important to use reasonable inlet profiles
in order to simulate a given backstep flow experiment. In the present study, the

FIGURE 1. Computed streamlines for DS experiment.

inlet profiles were obtained by the following procedure: (1) obtain the displacement thickness δ^* and the Reynolds number Re, based on the reference velocity U_o and the step height H, at the step from experimental data; (2) calculate the mean U-velocity, U_m, for the channel upstream of the step using the relation $U_m = U_o(1 - 2\delta^*{}_{in}/H_1)$, where H_1 is the channel height at the inlet of the domain; (3) run a channel calculation starting with a plug flow having mean velocity U_m at the inlet; (4) find the downstream location where the calculated displacement thickness δ^* matches $\delta^*{}_{in}$; and (5) use the channel solution at that location for the inlet boundary conditions for the backward-facing step flow problems. This amounts to computing the inlet section independently of the backstep region.

After grid independence testing, the selected grids consisted of 140 uniformly expanding grid lines in the streamwise direction and 140 (107 for JD's case) highly non-uniform grid lines in the transverse direction. The maximum expansion (or contraction) rates of the grid lines ranged from 8 to 10% depending on the case. This high non-uniformity of the grid is due to the high density of the grid lines in the near-wall regions and in the mixing layer at the top of the step in order to resolve the viscous layer: the first grid point off the wall is at $y^+ \leq 0.5$, where the wall unit y^+ is defined as $y^+ \equiv yu_\tau/\nu$, $u_\tau = \sqrt{\tau_w/\rho}$ and τ_w is the wall shear stress.

Figure 1 shows calculated streamlines for the DS case (with zero deflection angle of the top wall). The sharp discontinuity of the backward-facing step geometry produces a strong shear layer near the step. A large recirculation region is formed underneath the shear layer, which, in turn, creates a small corner eddy. As the shear layer spreads, it impinges on the bottom wall near the reattachment point X_r. Some of the impinging shear layer goes downstream and starts to develop into a boundary layer (the redeveloping boundary layer). Notice that the present streamline plot does not show an unrealistic behavior of the separation streamline near the reattachment point: Lasher and Taulbee[2] observed that the separation streamline was pulled back underneath the recirculating region when a fine grid was used in the near-wall region. We used a fine grid and did not observe that spurious behavior.

Figures 2(a), 2(b) and 2(c) show calculated skin friction coefficients C_f for JD, DS and KKJ cases, compared with corresponding experimental and DNS data. In all three cases, the model calculations underpredict the negative peak values of C_f
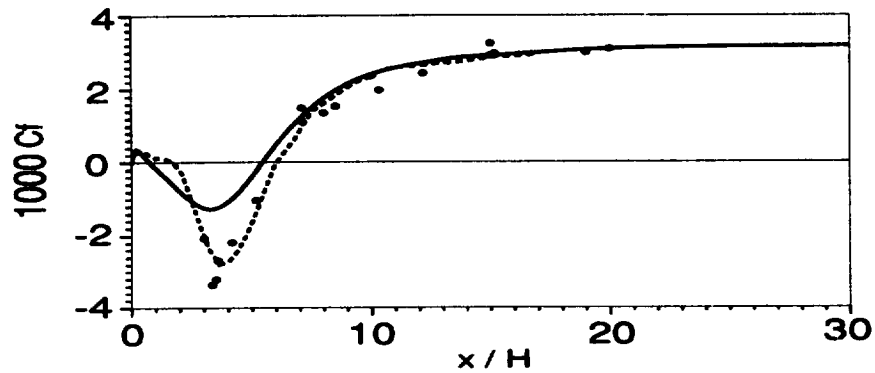
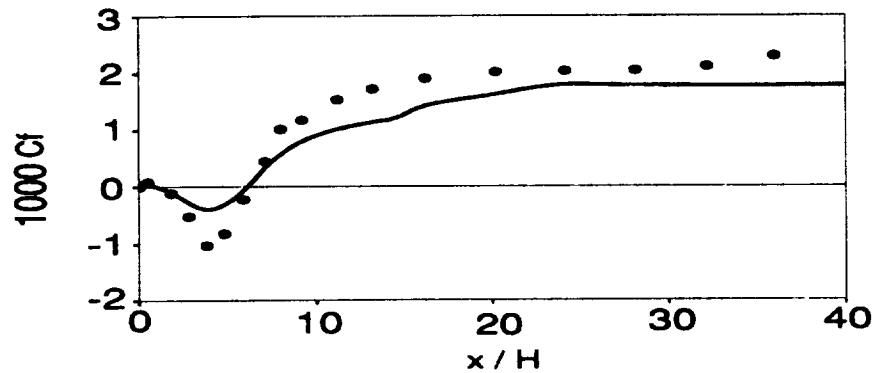FIGURE 2A. Skin friction coefficients: ● : JD experiment; ——: NRSM; - - -: DNS.

FIGURE 2B. Skin friction coefficients: ● : DS experiment; ——: NRSM.

in the recirculation zones. Also, for DS and KKJ cases (Figs. 2(b) and 2(c)), the calculated C_f is significantly below the experimental data in the regions downstream of X_r, which means slow and weak recovery of the redeveloping boundary layer.

In all three cases, the model underpredicts the negative peak values of C_f in the recirculation zones. In the DS and KKJ cases (Figs. 2(b) and 2(c)), the calculated C_f is significantly below the experimental data in the regions downstream of X_r, which means slow and weak recovery of the redeveloping boundary layer. It is interesting to note that, for JD's low Reynolds number case (Fig. 2(a)), the negative peak of the measured C_f in the recirculation region is comparable in magnitude to that in the redeveloping boundary layer region downstream of the reattachment point.

Surface pressure coefficients C_p ($\equiv 2(P - P_o)/(\rho U_o^2)$) are shown in Figs. 3(a), 3(b) and 3(c) for the three cases. With minor deviation, the calculations show fairly
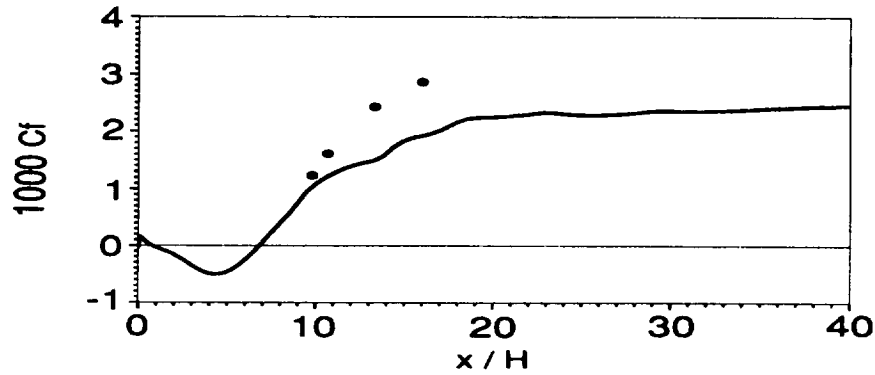
FIGURE 2C.   Skin friction coefficients: ● : KKJ experiment; ———: NRSM.

good agreement with the measurements for the JD and DS cases. The agreement for the KKJ case (Fig. 3(c)) is the worst.

Figures 4(a), 4(b) and 4(c) show mean U-velocity profiles at various positions upstream and downstream of the reattachment point, compared with experimental data of JD, DS and KKJ, correspondingly. Overall, the agreement of the computation with the experimental data is very good. For the JD case (Fig. 4(a)), the computed U-velocity profile at $x/H = 4$ shows insufficient backflow in the recirculation region, but otherwise the model predicts the redeveloping boundary layer almost perfectly. For the higher Re cases, the computations predict not only weak separated regions but also slow recovery of the redeveloping boundary layers downstream of X_r. This finding suggests that low Re DNS data might not be suitable for developing turbulence models that are mainly used for high Re flows.

Figures 5(a), 5(b) and 5(c) show computed profiles of the Reynolds stress components $\overline{u^2}$, $\overline{v^2}$, $-\overline{uv}$, at various positions upstream and downstream of the reattachment point, compared with JD's experimental data and LM's DNS data. It is quite encouraging to see that all three Reynolds stress profiles at the step, obtained from the channel flow solution with Re and δ^* matched to the experiment, show excellent agreement with the experimental data. Thus the inlet conditions computed with the model are in accord with experiment. In Fig. 5(a), the $\overline{u^2}$ profiles at $x/H = 4$ and 6 represent the dominance of the shear layer. At $x/H = 10$, JD's experimental data already show double peaks of the $\overline{u^2}$ profile, one peak being very near the wall. In the DNS and the model computations, the wall peak emerges further downstream, as shown in the profiles at $x/H = 19$. In addition, the $\overline{u^2}$ profiles at $x/H = 19$ indicate that the redeveloping boundary layer is not fully recovered from the free shear layer. The agreement between the calculated and the measured $\overline{v^2}$ profiles in Fig. 5(b) is as good as that between the DNS data and the measurements. In Fig. 5(c), the model calculations overpredict the peak values of $-\overline{uv}$ in the region near the reattachment point, while the DNS underpredicts them.

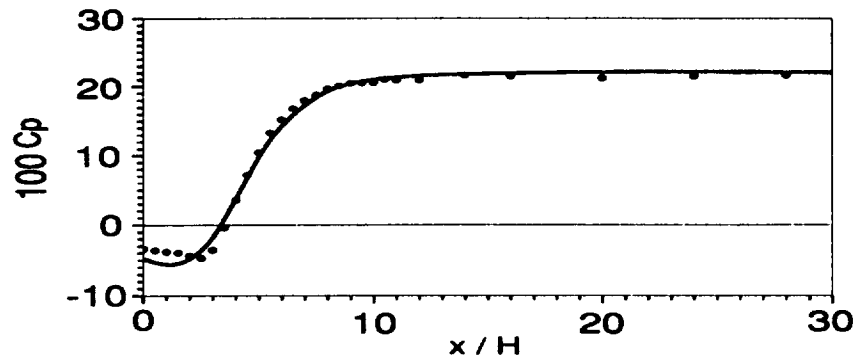The calculated Reynolds shear stress, $\overline{uv}$, is compared with DS's experimental

S. H. Ko

FIGURE 3A.   Surface pressure coefficients for JD case: ——, NRSM; •, experimental data.
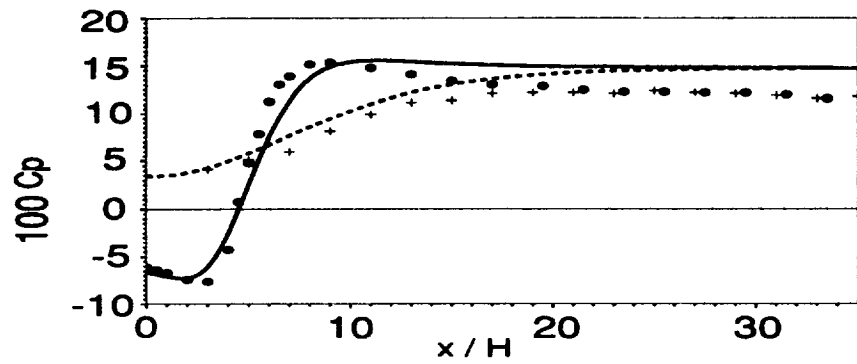

FIGURE 3B.   Surface pressure coefficients for DS case: ——, •, step-wall; - - -, +, opposite-wall. Symbols: experiment; lines: NRSM.
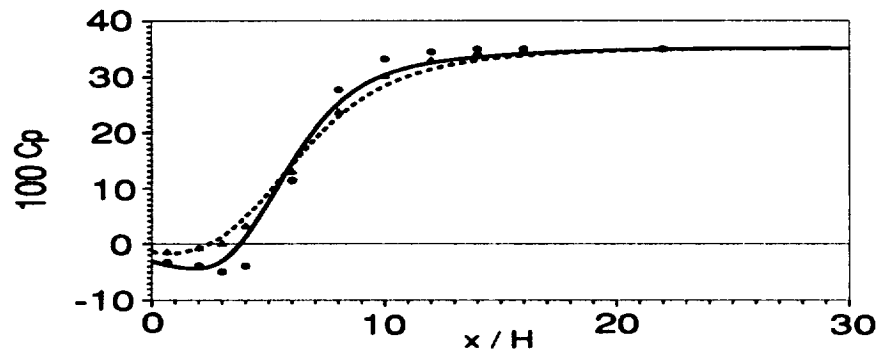

FIGURE 3C.   Surface pressure coefficients for KKJ case: ——, •, step-wall; - - -, ▲ , opposite-wall. Symbols: experiment; lines: NRSM.
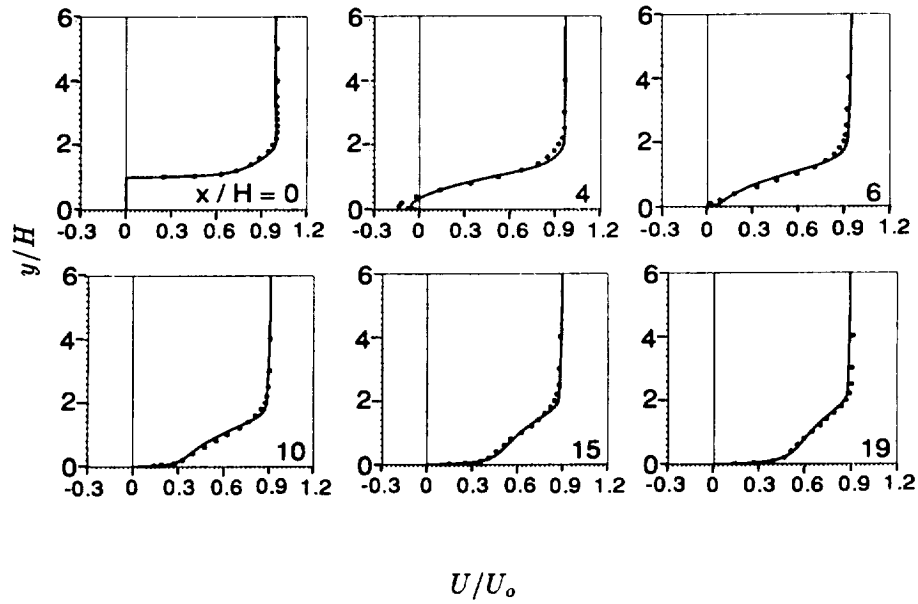
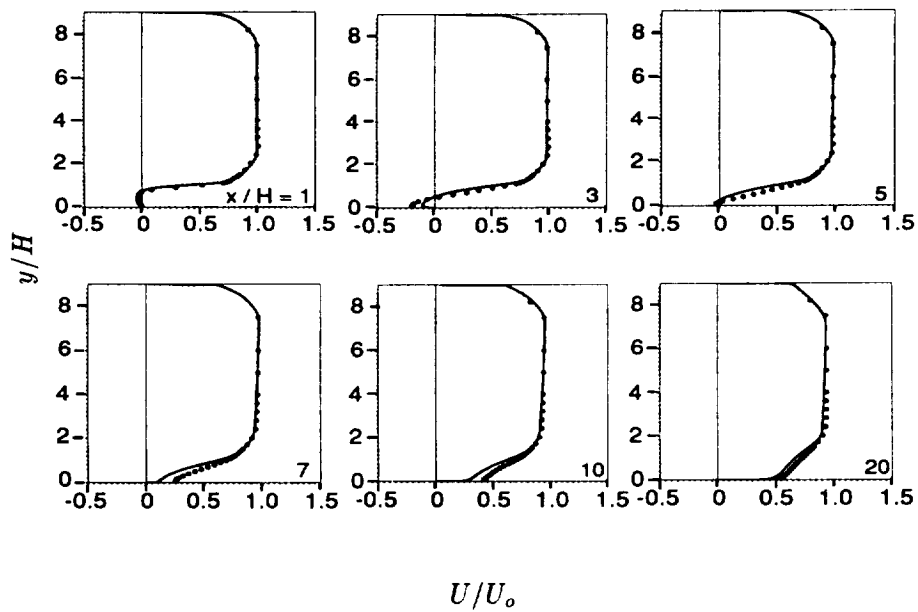FIGURE 4A. Mean U-velocity profiles for JD case. ● : experiment; ——: NRSM.

FIGURE 4B. Mean U-velocity profiles for DS case. ● : experiment; ——: NRSM.
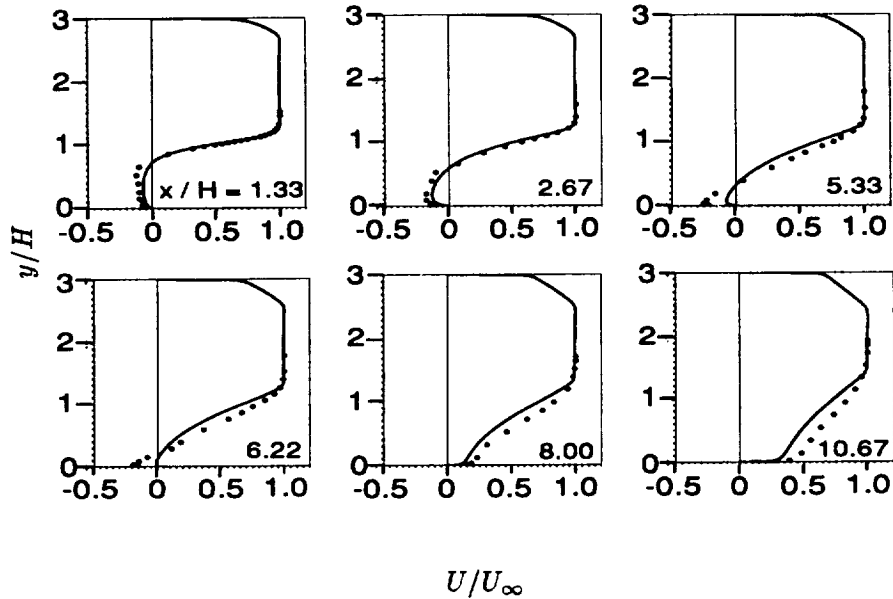
U/U_∞

FIGURE 4C. Mean U-velocity profiles for KKJ case. • : experiment; ———: NRSM.

data in Fig. 6. The calculated $\overline{uv}$ profiles at $x/H = 7$ and 10 show the peaks overpredicted by nearly 50%. In the recirculation region, the calculations show the peaks located higher than the experimental data.

Figures 7(a), 7(b), and 7(c) show the calculated budgets of the transport equations of U-velocity, k, and $\overline{uv}$ at four different positions upstream and downstream of the reattachment point, compared with LM's DNS data. Lines represent the model calculation and the symbols are the DNS data. Note that all the terms in the equations were normalized by the reference velocity U_o and the step height H, and then multiplied by 100.

In Figure 7(a), the convection term $-U_k \partial U/\partial x_k$ is balanced by the sum of the Reynolds stress gradient $\partial(-\overline{uu_k})/\partial x_k$ and the pressure gradient $-\partial P/\partial x$. Since the Reynolds stress gradient is the only term through which the turbulence acts on the mean momentum, it is quite important to understand the meaning of the profiles of $\partial(-\overline{uu_k})/\partial x_k$. The fact that at $x/H = 2$ the $\partial(-\overline{uu_k})/\partial x_k$ profiles change from being negative to being positive around $y/H = 1$ shows that momentum is being transferred by the turbulence from the shear layer to the flow in the wall region. As figure 7(a) reveals, the major deviation in the $\partial(-\overline{uu_k})/\partial x_k$ profiles is found in the negative peak levels. The viscous diffusion terms $\nu\nabla^2 k$ is negligible everywhere except in the region very near the wall. Notice that at $x/H = 2$ the calculation shows negative $-\partial P/\partial x$ while the DNS data shows positive $-\partial P/\partial x$. This deviation in $-\partial P/\partial x$ seems to be responsible for the deviation in the convection terms. As the flow goes downstream, the agreement between the model computation and the
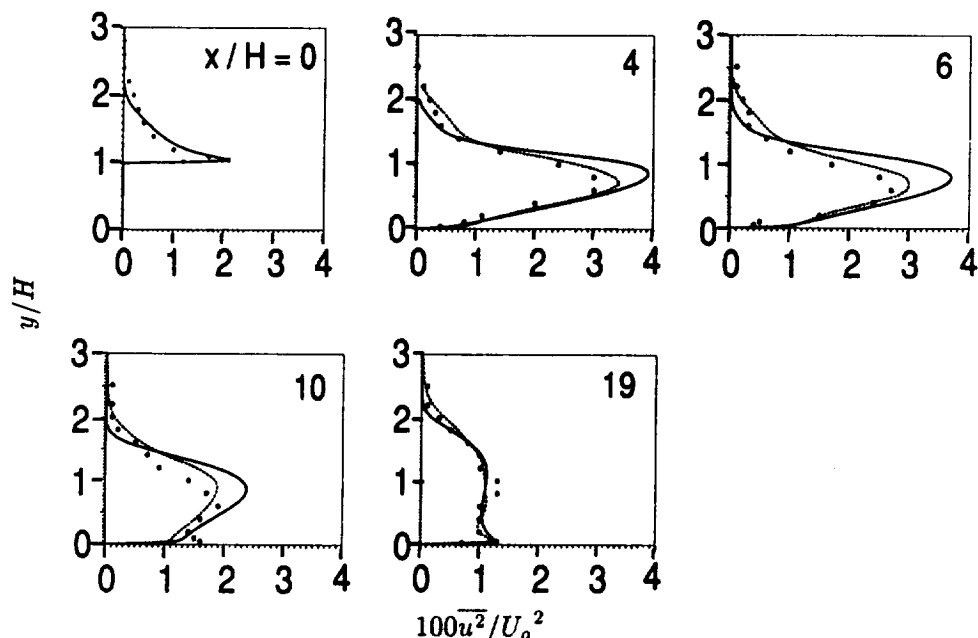
FIGURE 5A.   Reynolds stress $\overline{u^2}$ profiles for JD case: ———, NRSM; - - -, DNS; •, experimental data.

DNS data gets better. In fact, the agreement is very good at $x/H = 10$ where the $-\partial P/\partial x$ term is negligible.

As shown in Fig. 7(b), the production rate $\mathcal{P}$ in the transport equation of the turbulence kinetic energy is balanced mainly by the sum of the dissipation rate ϵ, the convection $-U_m \partial k/\partial x_m$ and the turbulent diffusion $\partial/\partial x_m \{\nu_{ml}/\sigma_k (\partial k/\partial x_l)\}$. The viscous diffusion $\partial/\partial x_m \{\nu(\partial k/\partial x_l)\}$ is negligible everywhere. Notice from the profiles of the turbulent diffusion that the turbulence kinetic energy is extracted from the middle of the shear layer and then transferred to the outer regions of the shear layer. Overall, the model calculation shows very good agreement with the DNS data.

In the budget of the $\overline{uv}$ transport equation, shown in Fig. 7(c), the production rate $\mathcal{P}_{12}$ is balanced by the sum of the redistribution F_{12} and the turbulent diffusion, according to the DNS data. However, the model calculation shows that the contribution from the turbulent diffusion is somewhat smaller than that from the anisotropic dissipation. In fact, the underprediction of turbulent diffusion seems to be the major deficiency of the present computation. The NRSM employs the simple gradient-diffusion hypothesis of Daly & Harlow (Durbin, 1993) for the triple velocity correlations. A more sophisticated formula for the triple velocity correlations may improve the model predictions.
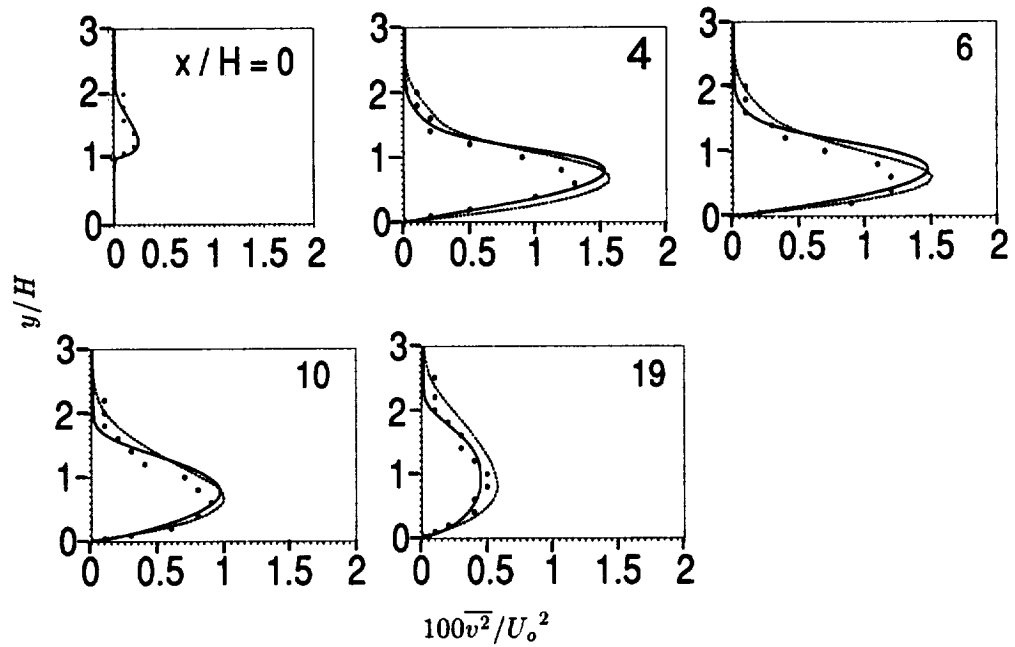
FIGURE 5B.   Reynolds stress $\overline{v^2}$ profiles for JD case: ——, NRSM; - - -, DNS; •, experimental data.
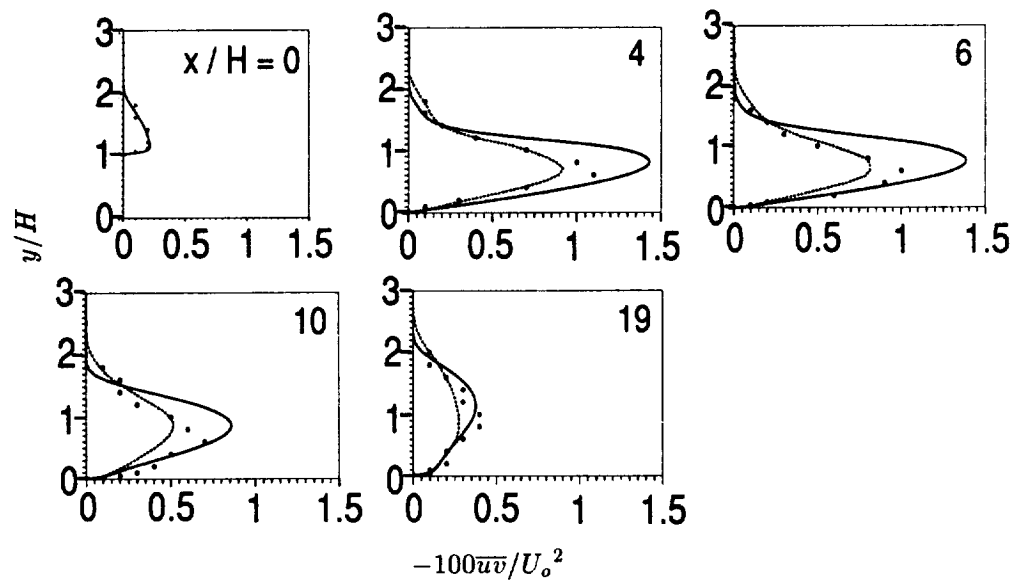

FIGURE 5C.   Reynolds stress $-\overline{uv}$ profiles for JD case: ——, NRSM; - - -, DNS; •, experimental data.
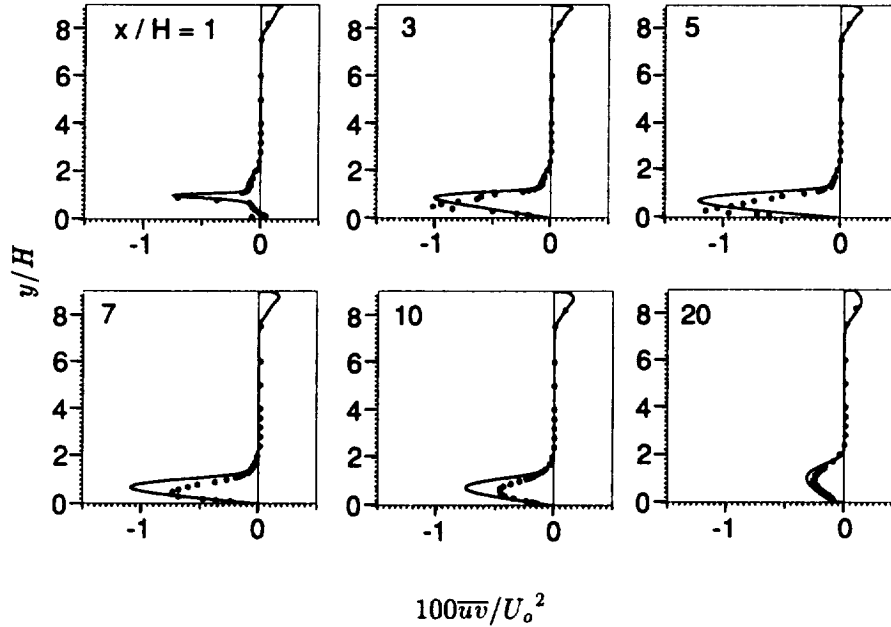
$$100\overline{uv}/U_o{}^2$$

FIGURE 6.   Reynolds stress $\overline{uv}$ profiles for DS case: ● : experiment; ———: NRSM.

2.2. Turbulent flow over forward-facing step

Turbulent flows over block-like structures are observed in a number of important engineering applications such as vehicles, buildings, and electronic chips. Understanding the flowfields over the forward-facing step will enhance the design of such applications. In addition, the forward-facing step flow provides an example of pressure-driven separation in a well characterized geometry.

Experimental data reported by Moss & Baker (1980) will be used for comparison. The contraction ratio H_1/H_2 is 10/11 and the Reynolds number, based on the step height H and the reference velocity U_o, is 46,000. The inlet of the computational domain is $10H$ upstream of the step ($x/H = 0$) and the exit is located $40H$ downstream of the step.

A computed streamline plot near the step is shown in Figure 8. As the boundary layer approaches to the step, it undergoes an adverse pressure gradient due to the presence of the step. The boundary layer separates at some distance upstream of the step, forming a corner separation bubble. Due to the sharp edge of the step, a secondary separation bubble occurs on the top surface of the lower wall downstream of the step. The length and height of the corner separation bubble predicted by the model computation are 1.0 H and 0.45 H whereas those given by the experimental data are 1.1 H and 0.6 H, correspondingly. Also, the predicted length of the secondary bubble is 5.5 H while the measured one is 4.8 H.

Figure 9 shows the calculated and measured profiles of the surface pressure coefficient C_p ($\equiv 2(P-P_o)/\rho U_o{}^2$) for the stepped wall. For the reference pressure P_o, the
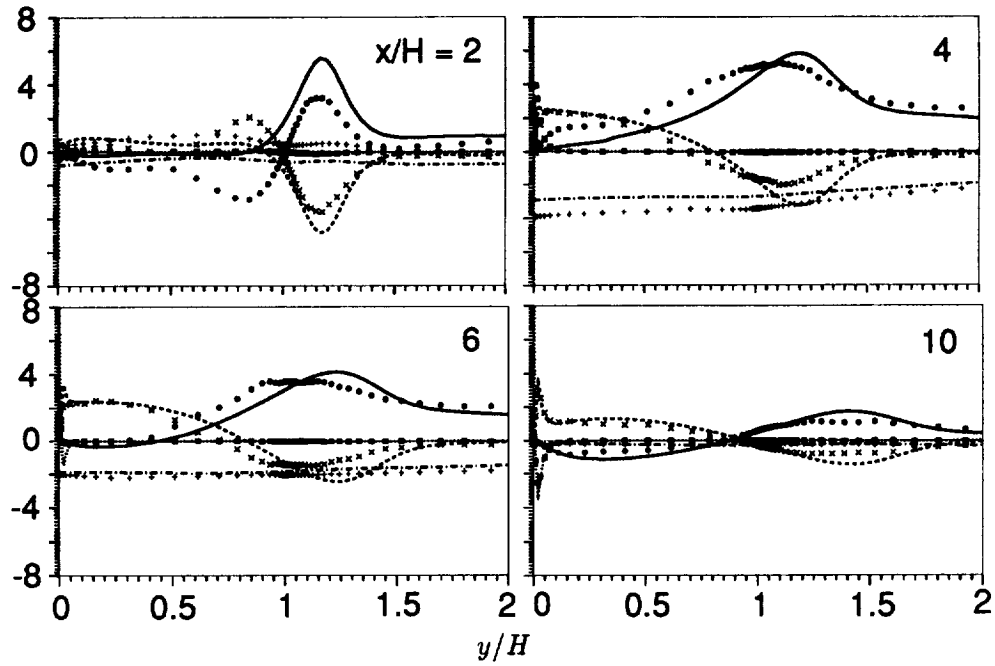
FIGURE 7A.   Budgets of the mean U-momentum equation for JD case: ———, •, $-U_k\partial U/\partial x_k$; — - —, +, $-\partial P/\partial x$; - - -, ×, $\partial(-\overline{uu_k})/\partial x_k$; - - -, ■, $\nu\partial/\partial x_k(\partial U/\partial x_k)$. Symbols: DNS; lines: NRSM
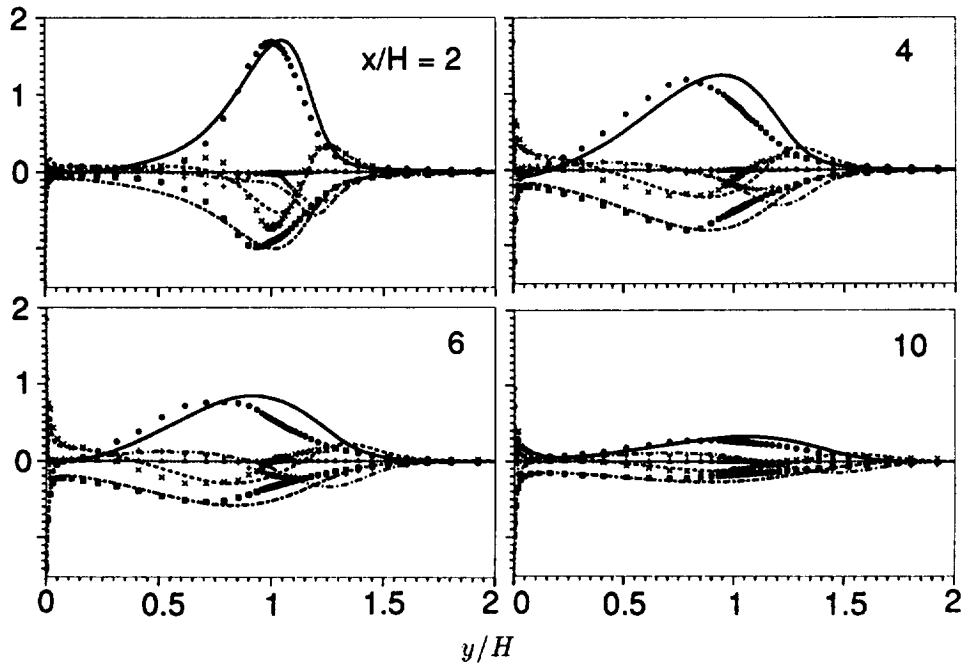

FIGURE 7B.   Budgets of the k-equation for JD case: — - —, +, $-U_m\partial k/\partial x_m$; ———, •, $\mathcal{P}$; — - —, ■, ϵ; - - -, $\triangle$, $\nu\nabla^2 k$; - - -, ×, $\partial/\partial x_m\{\nu_{ml}/\sigma_k(\partial k/\partial x_l)\}$. Symbols: DNS; lines: NRSM

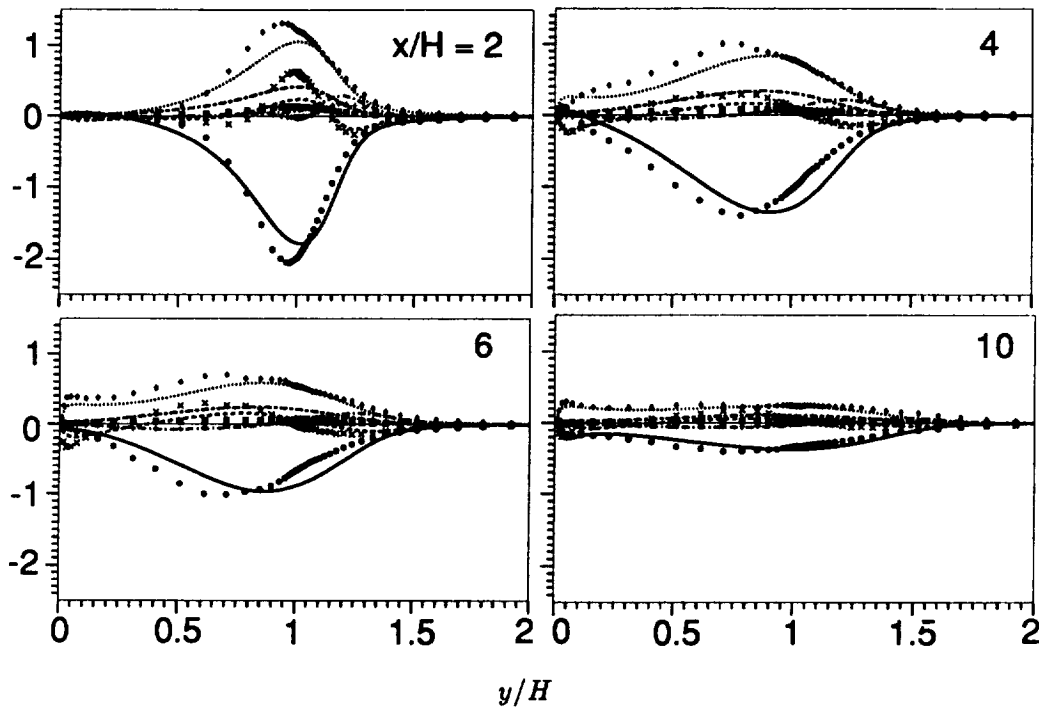FIGURE 7C.   Budgets of the $\overline{uv}$-equation for JD case: — · —, $+$, $-U_m \partial \overline{uv}/\partial x_m$; ———, $\bullet$, $\mathcal{P}_{12}$; · · ·, $\diamond$, F_{12}; – – –, $\times$, $\partial/\partial x_m\{\nu_{ml}/\sigma_k(\partial \overline{uv}/\partial x_l)\}$; — – —, $\blacksquare$, $(\overline{uv}/k)\epsilon$. Symbols: DNS; lines: NRSM

freestream pressure at $x/H = -8$ was used. The calculation agrees very well with the measurement in the region upstream of the step. As the approaching boundary layer decelerates in the corner separation region, C_p reaches its peak value of 0.52. Then C_p drops suddenly to -1.0 at the step, slowly recovering downstream of the step. Notice that the experimental data show a slight decrease in C_p in the region extending from the step to a couple of step heights downstream of the step where the computation shows a monotonic increase in C_p.

In Figure 10, the calculated profiles of the U-velocity at various measuring stations upstream and downstream of the step ($x = 0$) are compared with the experimental data. Notice that the boundary layer thickness of the approaching flow is comparable to the step height. As indicated in the profiles downstream of the step, the model calculation predicts a weak secondary separation bubble and slow recovery of the boundary layer after the bubble. These findings are consistent with those for the backstep flow cases. Other than these deficiencies, the calculation is able to predict the separation of the forward-facing step flows reasonably well.

Finally, the profiles of the Reynolds stress $\overline{u^2}$ are plotted in Fig. 11 along with the measurements. The calculation agrees excellently with the measurements, quantitatively as well as qualitatively. The calculated and the measured y locations of the

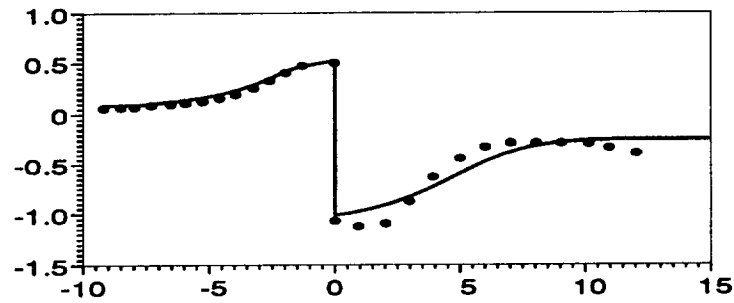FIGURE 8.   Computed streamlines for a forward-facing step flow.

FIGURE 9.   Surface pressure coefficients for a forward-facing step flow. ● : experiment (Moss & Baker); ———: NRSM.
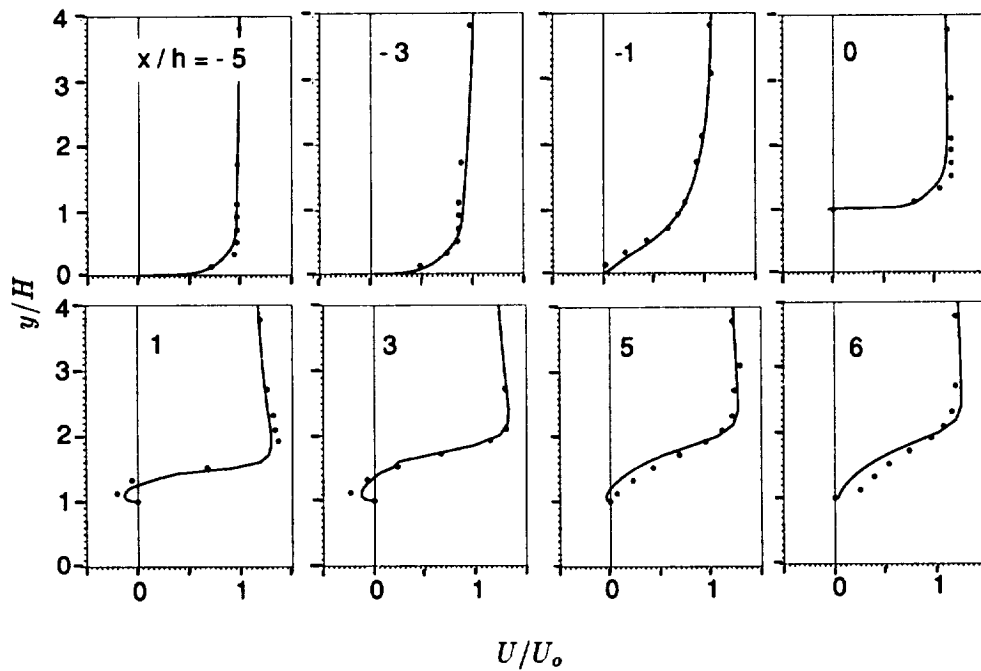

U/U_o

FIGURE 10.   Mean U-velocity profiles for a forward-facing step flow. ● : experiment (Moss & Baker); ———: NRSM.
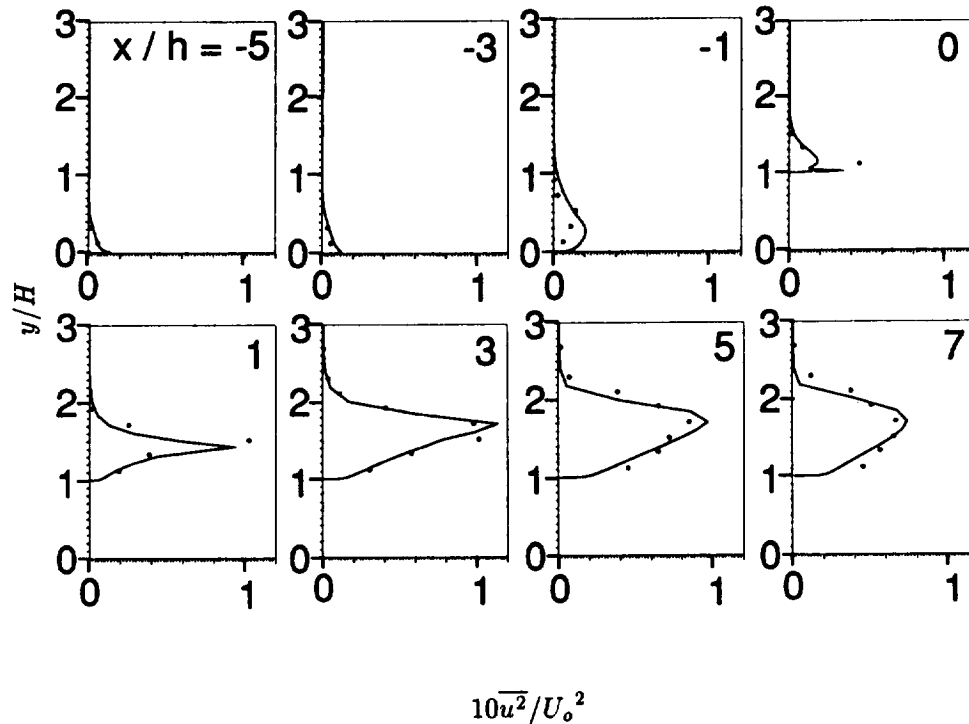
$$10\overline{u^2}/U_o{}^2$$

FIGURE 11.   Reynolds stress $\overline{u^2}$ profiles for a forward-facing step flow. • : experiment (Moss & Baker); ——: NRSM.

$\overline{u^2}$ peaks in the region downstream of the step are in good agreement, which implies that the calculation predicts the y location of the shear layer and the separation bubble correctly.

3. Summary

A near-wall Reynolds stress model (NRSM) has been used in numerical computations for two-dimensional, incompressible turbulent flows over backward and forward-facing steps. Numerical results were compared with Direct Numerical Simulation (DNS) data as well as experimental data for various flow quantities. The comparison reveals that the NRSM predicts the reattachment length fairly accurately. The NRSM also predicts the development of the boundary layer downstream of the reattachment point correctly when the Reynolds number is low. However, the model generally predicts a weak separation bubble and a slowly developing boundary layer when the Reynolds number is high. For more detailed comparison, budgets of the transport equations for the U-velocity, turbulence kinetic energy k, and the Reynolds shear stress $-\overline{uv}$ were calculated and compared with DNS data.

REFERENCES

BADRI NARAYANAN, M. A., KHADGI, Y. N. & VISWANATH, P. R. 1974 Similarities in pressure distribution in separated flow behind backward-facing steps. *The Aeronautical Quarterly.* **25**, 305-312.

BRADSHAW, P. & WONG, F. Y. F. 1972 The reattachment and relaxation of a turbulent shear layer. *J. Fluid Mech.* **52**, 113-135.

DRIVER, D. M. & SEEGMILLER, H. L. 1985 Features of a reattaching turbulent shear layer in divergent channel flow. *AIAA J.* **23**, 163-171.

DURBIN, P. A. 1991 Near-wall turbulence closure modeling without "damping functions". *Theoretical and Computational Fluid Dynamics.* **3**, 1-13.

DURBIN, P. A. 1993 A Reynolds stress model for near-wall turbulence. *J. Fluid Mech.* **249**, 465-498.

JOVIC, S. & DRIVER, D. M. 1993 Backward-facing step measurements at low Reynolds number. $Re_h = 5,000$. NASA TM to be published.

JOVIC, S. & DRIVER, D. M. 1993 Reynolds number effects on the skin-friction in separated flows behind a backward-facing step submitted for publication.

KIM, J., KLINE, S. J. & JOHNSTON, J. P. 1980 Investigation of a reattaching turbulent shear layer: flow over a backward-facing step. *J. Fluids Engr.* **102**, 302-308.

KO, S. 1993 Application of a Reynolds stress model to separating boundary layers. Annual Research Briefs-1992, Center for Turbulence Research, Stanford Univ./NASA Ames, 199-211.

KO, S. & DURBIN, P. A. 1993 Application of a near-Wall turbulence model to adverse pressure gradient and separating boundary layers. *Near-Wall Turbulent Flows*, edited by So *et al.*, Elsevier, 145-153.

LASHER, W. C. & TAULBEE, D. B. 1992 On the computation of turbulent backstep flow. *Int. J. Heat and Fluid Flow.* **13**, 30-40.

LE, H. AND MOIN, P. 1993 Direct numerical simulation of turbulent flow over a backward-facing step. Report TF-58,Thermosciences Division, Department of Mechanical Engr., Stanford University.

MOSS, W. D. & BAKER, S. 1980 Re-circulating flows associated with two-dimensional steps. *The Aeronautical Quarterly.* **31**, 151-172.

SIMPSON, R. L., CHEW, Y.-T., & SHIVAPRASAD, B. G. 1981 The structure of a separating turbulent boundary layer. Part 1. Mean flow and Reynolds stresses. *J. Fluid Mech.* **113**, 23-51.

THANGAM, S. & SPEZIALE, C. G. 1992 Turbulent flow past a backward-facing step: A critical evaluation of two-equation models. *AIAA J.* **30**, 1314-1320.

$C1-2$